



Supporting Information

for *Adv. Sci.*, DOI 10.1002/adv.202202414

Small Molecule NIR-II Dyes for Switchable Photoluminescence via Host –Guest Complexation and Supramolecular Assembly with Carbon Dots

*Dinabandhu Sar, Fatemeh Ostadhossein, Parikshit Moitra, Maha Alafeef and Dipanjan Pan**

Supporting Information

Small Molecule NIR-II Dyes for Switchable Photoluminescence via Host -Guest Complexation and Supramolecular Assembly with Carbon Dots

*Dinabandhu Sar,[†] Fatemeh Ostadhossein,[†] Parikshit Moitra,[†] Maha Alafeef and Dipanjan Pan**

Corresponding author: dipanjan@som.umaryland.edu

1. Experimental Section.**Materials and Methods.**

All the reagents and chemicals were purchased from well-known commercial vendors and used without further purification steps. Cucurbit[8]uril was procured from Sigma-Aldrich and milli-Q water was used throughout the experiments.

Synthetic Procedure of NIR-II Dyes.

Naphtho[1,2-c:5,6-c']bis[1,2,5]thiadiazole-5,10-diboronic acid bis(pinacol) ester, **1** (3.3 mmol), tetrakis(triphenylphosphine)palladium(0) (0.17 mmol), potassium carbonate (16.5 mmol) and 4-bromo-*N,N*-diarylaniline, **2** (8.2 mmol) were mixed and dissolved in anhydrous toluene (80 mL) and nitrogen-bubbled distilled water (10 mL). Either of 4-Bromotriphenylamine, **2a**, 4-Bromo-*N,N*-di-*p*-tolylaniline, **2b** or 4-Bromo-*N,N*-bis(4-methoxyphenyl)aniline, **2c**, was used as the bromo components to synthesize three different compounds. This solution was heated at 115 °C for 48 hours under nitrogen atmosphere. After the reaction time is over, the solvent was removed under reduced pressure and the resulting solid was dissolved in chloroform. This organic layer was washed with brine and filtered through anhydrous sodium sulphate. The filtrate was dried in a rotary evaporator and the crude product was purified by silica gel column chromatography with hexane/CHCl₃ as the eluent. This afforded the final compounds: 4,4'-(naphtho[1,2-c:5,6-c']bis([1,2,5]thiadiazole)-5,10-

diyl)bis(N,N-diphenylaniline), D₁AD₁, **3a** in 47% yield; 4,4'-(naphtho[1,2-c:5,6-c']bis([1,2,5]thiadiazole)-5,10-diyl)bis(N,N-di-p-tolylaniline), D₂AD₂, **3b** in 39% yield; 4,4'-(naphtho[1,2-c:5,6-c']bis([1,2,5]thiadiazole)-5,10-diyl)bis(N,N-bis(4-methoxyphenyl)aniline), D₃AD₃, **3c** in 51% yield.

Characterization of **3a**.

¹H NMR (400 MHz, CDCl₃, TMS, rt) δ (ppm) 9.01 (*m*, 2H), 8.91 (*d*, *J* = 8.0 Hz, 2H), 8.10 (*m*, 2H), 8.03 (*m*, 4H), 7.30 (*m*, 8H), 7.21 (*m*, 8H), 7.08 (*m*, 4H); ¹³C NMR (100 MHz, CDCl₃, TMS, rt) δ (ppm) 147.58, 130.48, 129.66, 127.66, 125.29, 124.48, 123.76, 122.90, 120.78. HRMS (*m/z*, ESI-MS, [M+H]⁺) Calcd. for C₄₆H₃₁N₆S₂ 731.2052, found 731.2014.

Characterization of **3b**.

¹H NMR (400 MHz, CDCl₃, TMS, rt) δ (ppm) 8.97 (*s*, 2H), 8.0 (*d*, *J* = 8.0 Hz, 4H), 7.19 (*d*, *J* = 8.0 Hz, 4H), 7.12 (*m*, 16H), 2.35 (*s*, 12H); ¹³C NMR (100 MHz, CDCl₃, TMS, rt) δ (ppm) 153.01, 147.84, 143.85, 132.18, 132.0, 129.0, 124.22, 123.22, 120.5, 30.41, 29.16, 28.68, 21.67, 19.86, 13.10. HRMS (*m/z*, ESI-MS, [M+K]⁺) Calcd. for C₅₀H₃₈KN₆S₂ 825.2236, found 825.3798.

Characterization of **3c**.

¹H NMR (400 MHz, CDCl₃, TMS, rt) δ (ppm) 8.95 (*s*, 2H), 7.98 (*d*, *J* = 8.0 Hz, 4H), 7.16 (*d*, *J* = 8.0 Hz, 8H), 7.10 (*d*, *J* = 8.0 Hz, 4H), 6.88 (*m*, 8H), 3.83 (*s*, 12H); ¹³C NMR (100 MHz, CDCl₃, TMS, rt) δ (ppm) 156.26, 154.04, 149.33, 140.46, 132.98, 130.03, 128.47, 127.16, 127.11, 124.96, 124.01, 119.68, 114.81, 55.52, 31.93, 30.19, 29.71, 29.37, 22.70, 14.19. HRMS (*m/z*, MALDI, [M+4H]⁺) Calcd. for C₅₀H₄₂N₆O₄S₂ 854.2709, found 854.5880.

Synthesis of Red Carbon Dot.

The synthesis of red carbon dot was carried out following a previously reported literature procedure.^[1] Briefly, equimolar amount of 2,5-diaminotoluene sulfate (100 M) and urea (100 M) were dissolved in 10 mL of milli-Q water and vortexed for 2 mins. The well suspended solution was then transferred to a teflon-lined autoclave for hydrothermal synthesis when the heating cycle was set to 150 °C for 8 h. After the required incubation time at elevated temperature, the vessel was brought down to room temperature, added with milli-Q water and centrifuged for 10 mins at 4200 rpm to remove the undesired contaminants. The nanoparticles were passed through two consecutive syringe filters (0.45 and 0.22 µm mesh size) and then dialyzed (MWCO = 2000 Da) against 1X PBS buffer (pH = 7.4). The suspension was kept at 4 °C for long term storage and tip sonicated briefly before each experiment.

UV-Visible Spectroscopy.

The UV-Visible spectra were recorded on Agilent Cary 5000 UV-Vis-NIR system.

Fluorescence Spectroscopy.

The fluorescence spectra were recorded on a Varian Cary 5G instrument. The 2D excitation–emission contours were obtained from a Horiba Aqualog scanning spectrofluorometer (Horiba Scientific, Edison, NJ).

NMR Spectroscopy.

The NMR spectra were collected on Varian VXR 500 (Varian, Inc., Palo Alto, CA) spectrometer operating at 400 MHz. The results were analyzed by MestRenova 11.0 (Mestrelab Research SL; Santiago de Compostela, Spain) software.

Mass Spectrometry.

Both the electrospray ionization (ESI) and matrix-assisted laser desorption/ionization (MALDI) quadrupole time of flight (Q-ToF) mass spectra were collected at mass spec facilities at UIUC.

FT-IR Spectroscopy.

The samples were drop casted and dried on MirrIR IR-reflective glass slides (Kevley Technologies, Chesterland, OH, USA). The thin films were then recorded in attenuated total reflectance (ATR) mode on a Nicolet Nexus 670 FT-IR instrument (ThermoFisher Scientific, Waltham, MA, US).

Scanning Electron Microscopy (SEM).

The samples were mounted on a SEM sample holder using a piece of carbon tape and then gold-coated via sputtering for 60 sec at 20 mA. The imaging was performed with an accelerating voltage of 10 kV, extracting current of 10 μ A and in a relatively long working distance of 25 mm. These SEM images were recorded with a Hitachi (Schaumburg, Illinois) S-4800 SEM with Oxford Instruments (Abingdon, Oxfordshire).

Transmission Electron Microscopy (TEM).

The TEM images were obtained using a TEM microscope (FEI) equipped with a Peltiercooled Tietz (TVIPS) $2k \times 2k$ charge-coupled device camera. 5 μ L of the diluted samples were deposited on a carbon-coated copper grid (TED PELLA Inc., Redding, CA) and kept for 5 minutes. The extra liquid was then removed with filter paper and the sample was dried overnight before imaging.

Atomic Force Microscopy (AFM).

The atomic force microscopy was performed in tapping mode with a Bruker MultiMode Nanoscope IIIA instrument (Billerica, MA). The diluted samples were deposited on a mica wafer fixed on a steel disc and the extra liquid was taken out after 5 mins. The disc was then vacuum dried for overnight.

X-ray Photoelectron Spectroscopy (XPS).

The carbon dots were drop cast over a glass slide and dried properly before the XPS measurement on a Physical Electronics PHI 5400 spectrometer using Al K α (1486.6 eV) radiation. The spectra were corrected to the C–C bond at 284.8 eV and the analyses were performed on CasaXPS software.^[2]

Docking Studies.

The chemical structures were first energy minimized using a general ab initio quantum chemistry package, General Atomic and Molecular Electronic Structure System (GAMESS) program.^[3] We used B3LYP functional while performing the density functional theoretical (DFT) calculations with 6-31G(d) as the basis set. Pople N31 was used for the polar groups. The energy minimized structures were then undertaken for docking studies using AutoDock 4.0 software.^[4]

HOMO-LUMO Calculations.

The chemical structures were initially energy optimized and the HOMO-LUMO surfaces were then calculated from their energy minimized geometries using GAMESS.^[3] We used B3LYP functional while performing the density functional theoretical (DFT) calculations with 6-31G(d) as the basis set. Pople N31 was used for the polar groups. The highest occupied molecular orbital (HOMO) and the lowest unoccupied molecular orbital (LUMO) was then

calculated from the energy minimized geometries. The HOMO and LUMO were also calculated for the docked geometries in a similar fashion.

Quantum yield measurements.

The quantum yields of the conjugates were measured according to the previously reported methods.^[5–7] UV-visible and fluorescence spectra of the DAD systems before and after the addition of CB and rCD were collected at five different concentrations. The maximum concentration of DAD systems was 200 μ M. The DAD+CB conjugates were prepared by mixing 200 μ M of DAD and 400 μ M of CB[8] solutions in DMSO. Further, DAD+CB+rCD conjugates were made with 200 μ M of DAD, 400 μ M of CB[8] solutions in DMSO and 1 mg/mL solution of rCD in water. These solutions were then diluted sequentially to obtain five different concentrations for quantum yield measurements.

Integrated fluorescence intensities were calculated and plotted against the absorbances recorded at the excitation wavelength for five different concentrations. The curves were linear fitted and the slopes of the curves were used to calculate quantum yield of the respective systems. The following equation was used to calculate the quantum yields.

$$QY_X = QY_{ST} \times \left(\frac{Slope_X}{Slope_{ST}} \right) \times \left(\frac{RI_X^2}{RI_{ST}^2} \right)$$

Here, QY_X and QY_{ST} are the quantum yields for the sample and standard, IR-26 dye respectively. RI_X and RI_{ST} are the refractive indexes for the solvents used for suspending sample and standard respectively. A reference near-infrared fluorophore, IR-26 ($QY = 0.5\%$), was used to calculate the quantum yields.

Measurement of hydrodynamic diameter.

A DMSO stock solution of the NIR-II dye (1 mM) was first prepared and mixed with a DMSO stock solution of CB[8] (2 mM) to form the inclusion complex (photoluminescence ‘ON’). This

supramolecular host-guest complex was further incubated with a 5 mg/mL water solution of rCD (photoluminescence ‘OFF’). This solution was then diluted at least 100 times with milli-Q water before any measurement. The average hydrodynamic diameter of these particles was then monitored with a particle tracking analyzer (Zetaview Particle Metrix). An average of 10 such measurements was represented in each case. The machine cell was adequately cleaned before each use.

MTT based cellular viability assay.

HEK293 cells were cultured in DMEM high glucose media with 10% FBS supplement. Cells were maintained and passaged at required intervals with 0.25% trypsin-EDTA media. Cytotoxicity of the three NIR-II dye conjugates (before and after the addition of CB[8] and rCD) at different concentrations was determined using MTT assay. A stock solution of NIR-II dye (10 mM), CB[8] (20 mM) and rCD (50 mg/mL) was used for preparing the suspensions of definite concentrations.

In brief, 20000 cells per well were plated in 96 well plate and allowed to grow till 70-80% confluency. After 24 h, the cells were treated with different concentrations of the conjugates for 6 h. After the incubation period, the media was removed, and the cells were added with fresh media. After another 42 h of incubation, 20 μ L of MTT (5 mg/mL stock concentration) was added to the wells for 4 h. The media was finally removed and added with 200 μ L of DMSO. The % cellular viability was then calculated as,

$$\% \text{ Cellular viability} = \left[\frac{(A_{570} (\text{treated cells}) - A_{570} (\text{DMSO}))}{(A_{570} (\text{non-treated cells}) - A_{570} (\text{DMSO}))} \right] \times 100$$

Blood smear experiment.

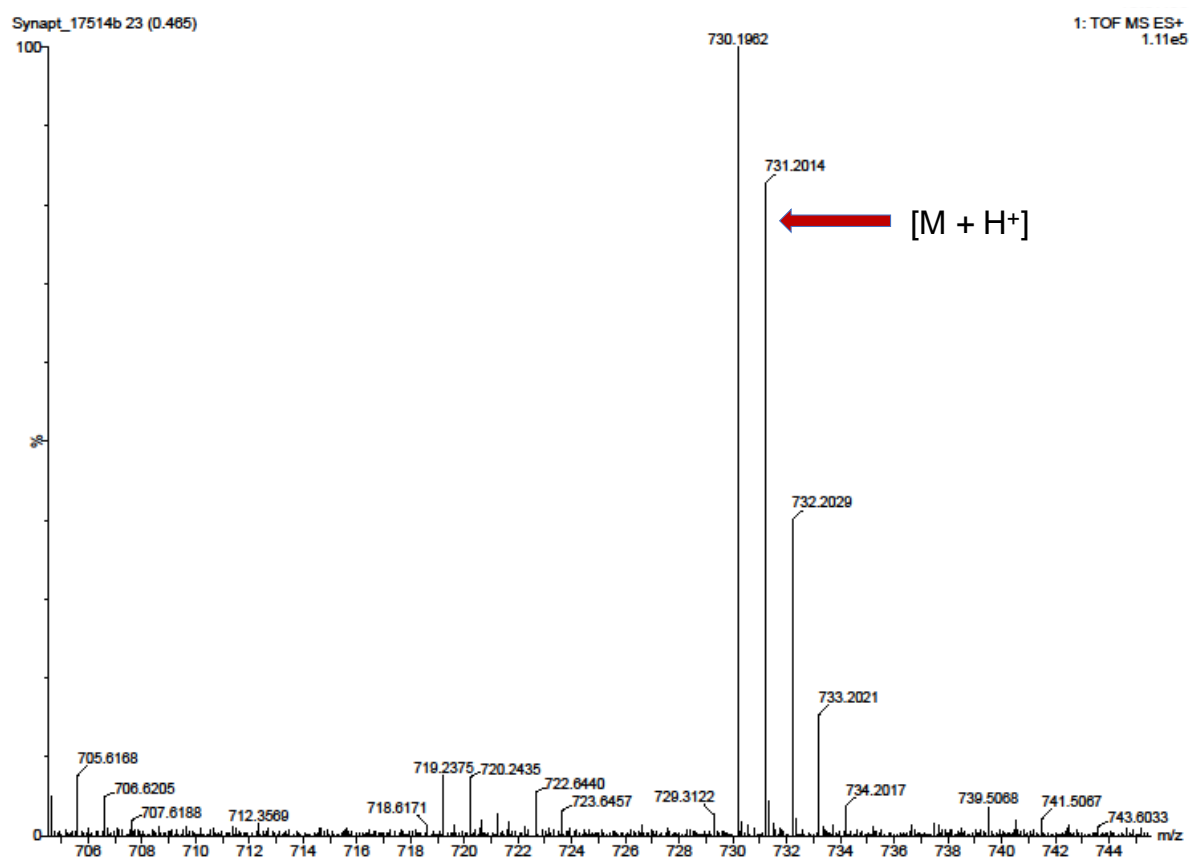
The protocol was followed from a previously reported literature protocol.^[8] Human blood was incubated with 400 μ M of D₃AD₃, 800 μ M of CB[8] and 2 mg/mL solution of rCD in 1X PBS.

The blood samples were then diluted 5 times, allowed to air-dry for 1-2 mins over a glass slide added with a coverslip before being imaged under bright field Nikon Ti2 inverted microscope (100x).

NIR-II imaging studies.

A BALB/c mouse was sacrificed and injected with the turn-ON photoluminescent complex, D₃AD₃+CB[8], for *ex vivo* NIR-II bioimaging. The inclusion complex was made with 400 μ M of D₃AD₃ and 800 μ M of CB[8]. 20 μ L of this suspension were then injected either to heart or colon or under the skin tissue and incubated for 30 mins at room temperature. The tissues were then imaged immediately under Nikon Ti2-E Inverted Automated Research Microscope. For NIR-II imaging, NIRvana 640ST camera was used. ET850/40x Chroma ET Series excitation filter and ET1300/100m Emission Filter 25mm with custom 50/50 beam splitter was used for NIR-II microscopic imaging.

2. Figures.

**Figure S1.** HRMS of D₁AD₁ compound.

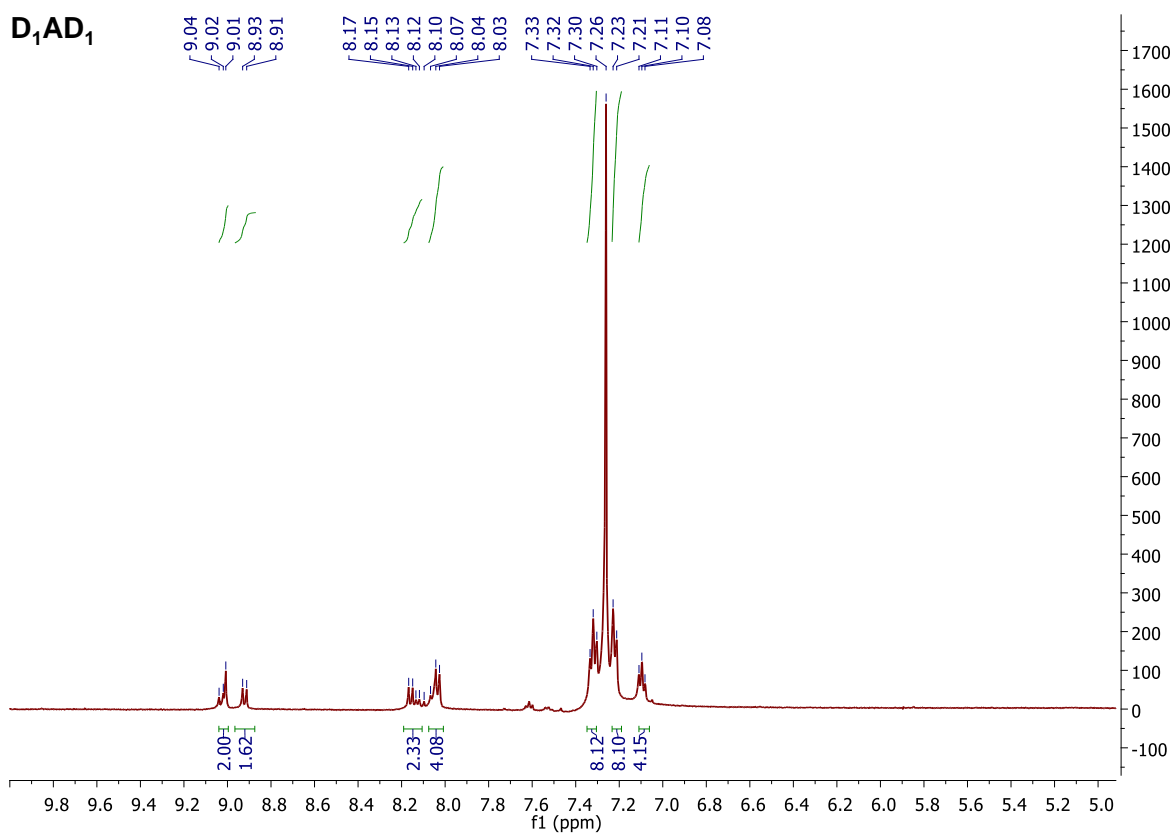


Figure S2. ^1H -NMR spectrum of D₁AD₁ compound.

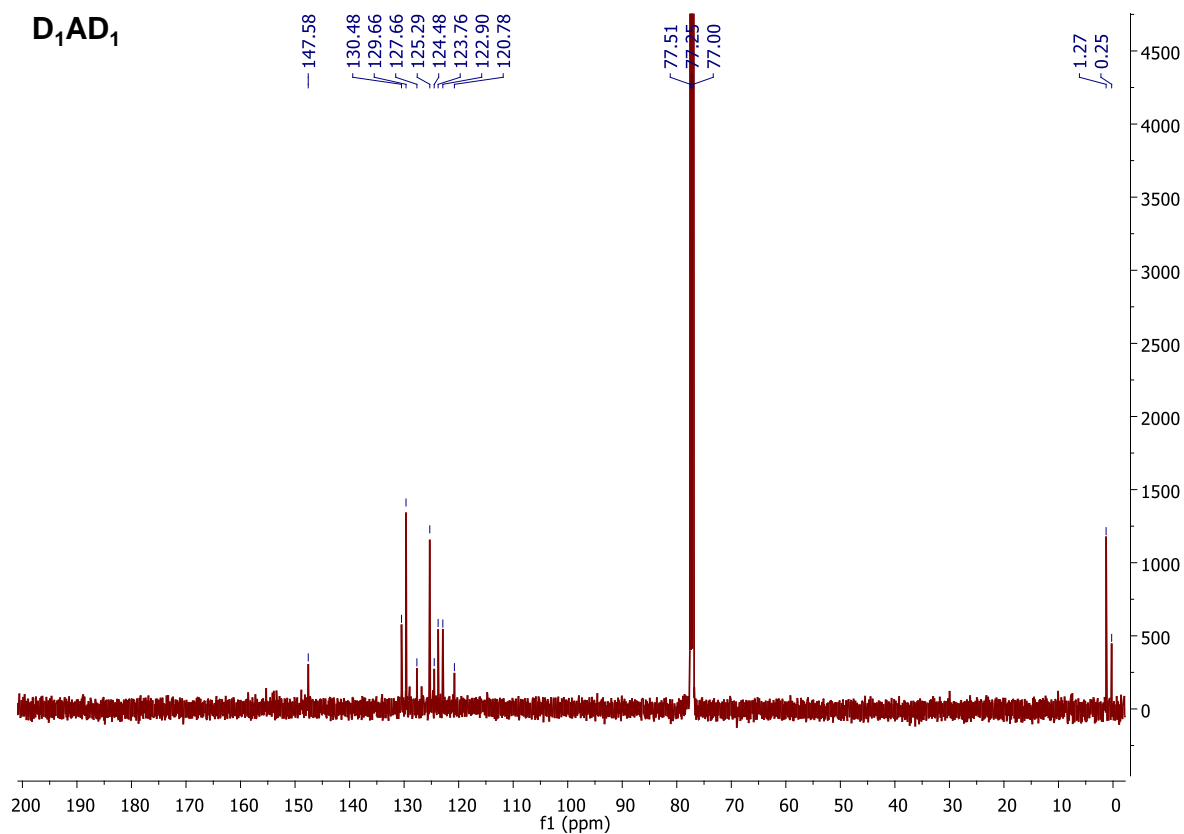


Figure S3. ^{13}C -NMR spectrum of D₁AD₁ compound.

Single Mass Analysis

Tolerance = 5.0 PPM / DBE: min = -1.5, max = 100.0

Element prediction: Off

Number of isotope peaks used for i-FIT = 3

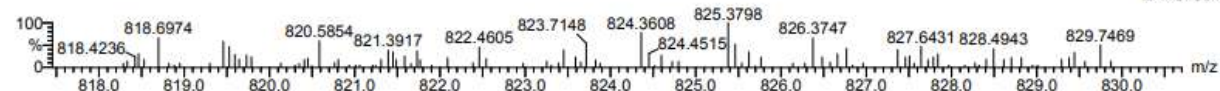
HRMS of D₂AD₂ m/z (M + K⁺) = 825.3798

Monoisotopic Mass, Even Electron Ions

478 formula(e) evaluated with 1 results within limits (up to 50 closest results for each mass)

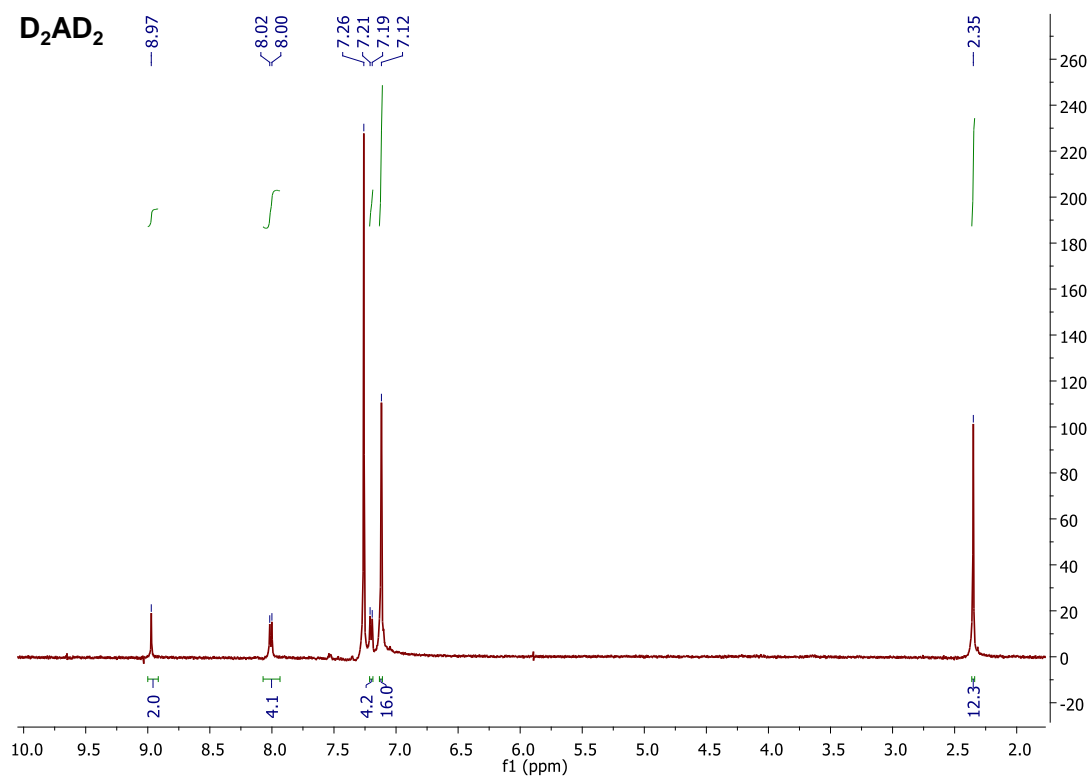
20191212-1

Qtof_73316a 91 (3.450) AM (Cen,5, 80.00, Ar,14000.0,558.36,0.70,LS 5); Sm (SG, 2x5.00); Cm (91:107)

1: TOF MS ES+
2.44e+001

Minimum: -1.5
Maximum: 5.0 5.0 100.0

Mass	Calc. Mass	mDa	PPM	DBE	i-FIT	Formula
825.3798	825.3773	2.5	3.0	29.5	0.4	C52 H53 N6 S2

Figure S4. HRMS of D₂AD₂ compound.**Figure S5.** ¹H-NMR spectrum of D₂AD₂ compound.

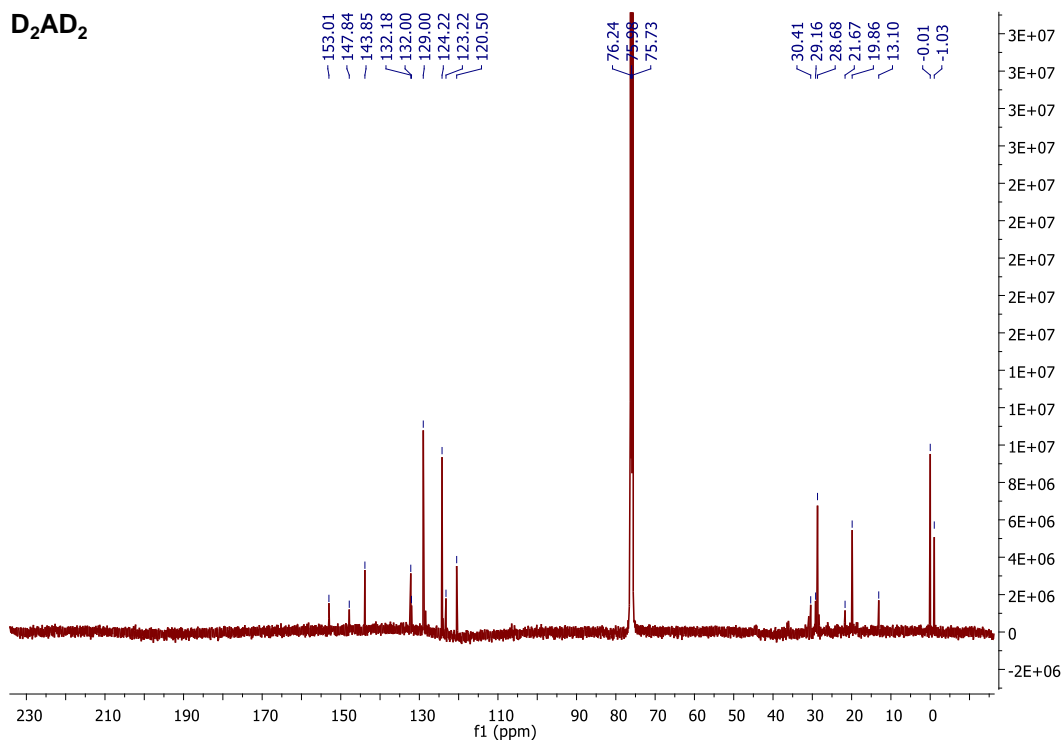


Figure S6. ¹³C-NMR spectrum of D₂AD₂ compound.

Single Mass Analysis

Tolerance = 5.0 PPM / DBE: min = -1.5, max = 100.0

Element prediction: Off

Number of isotope peaks used for i-FIT = 3

Monoisotopic Mass, Even Electron Ions

4659 formula(e) evaluated with 20 results within limits (up to 50 closest results for each mass)

HRMS of D₃AD₃

m/z (M + 4H⁺) = 854.5880

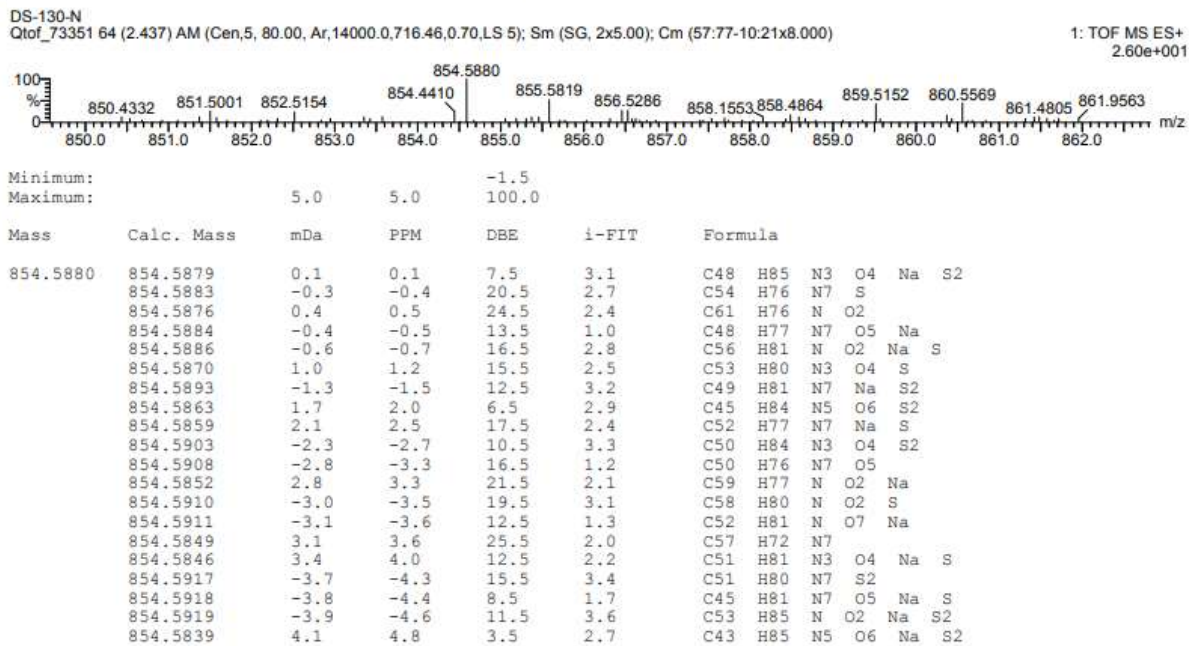


Figure S7. HRMS of D₃AD₃ compound.

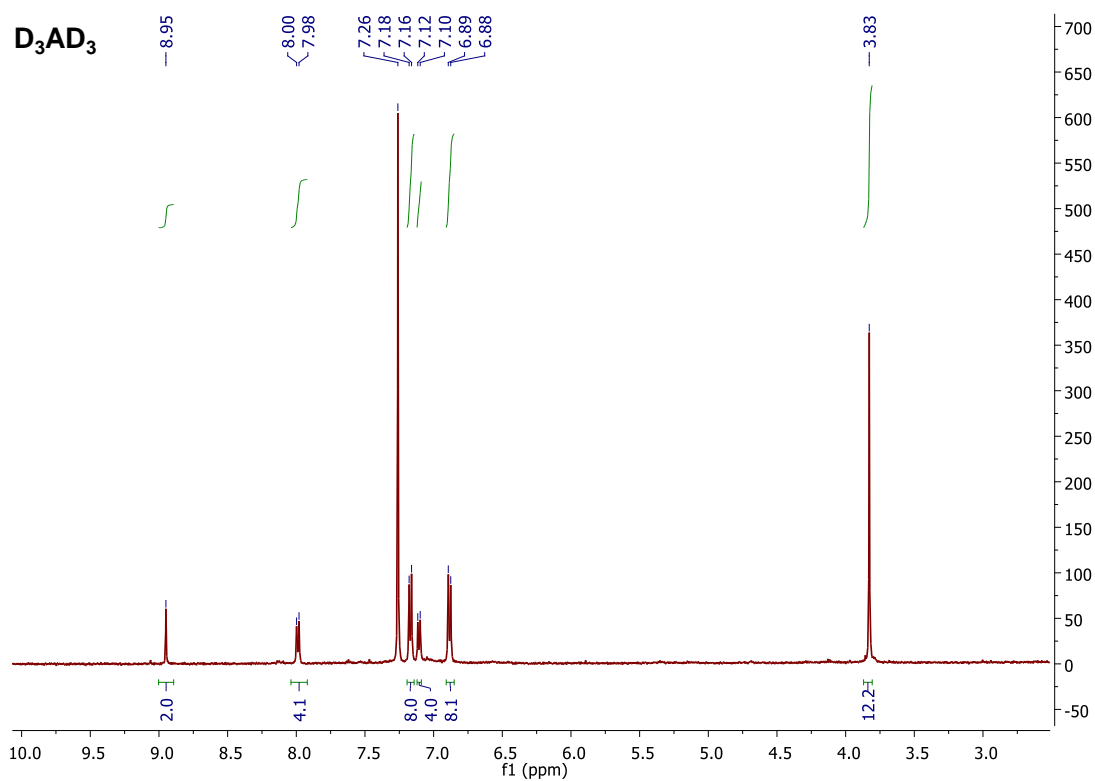


Figure S8. ¹H-NMR spectrum of D₃AD₃ compound.

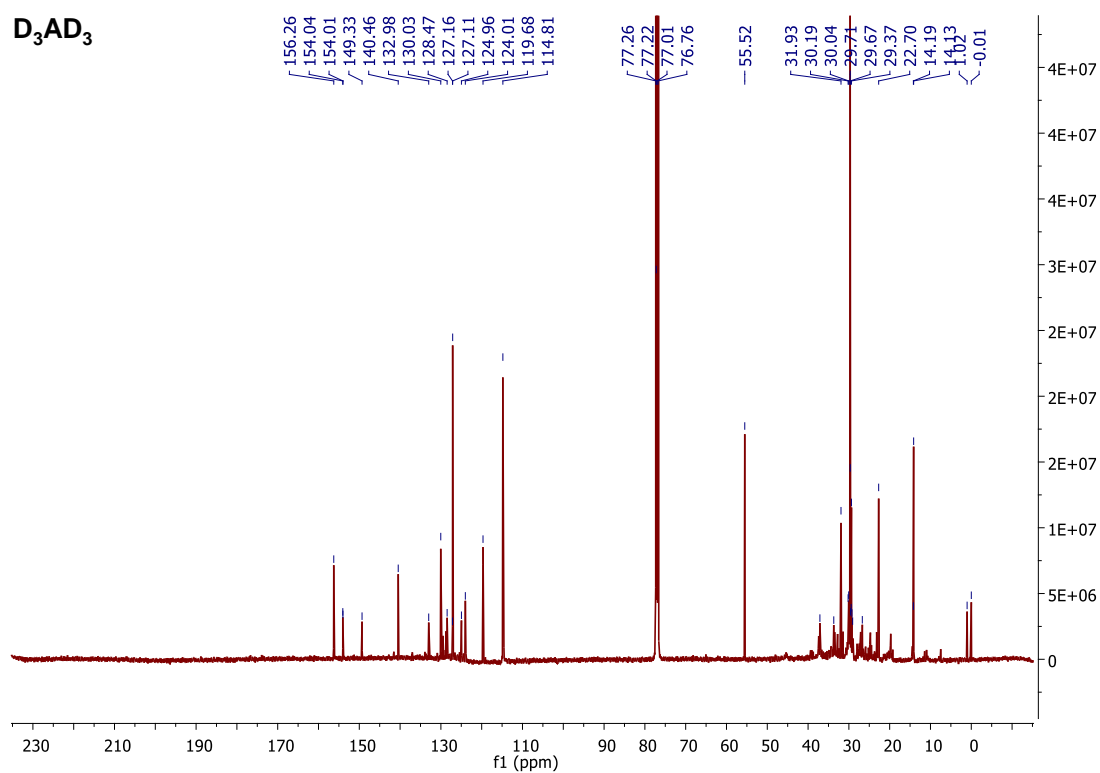


Figure S9. ¹³C-NMR spectrum of D₃AD₃ compound.

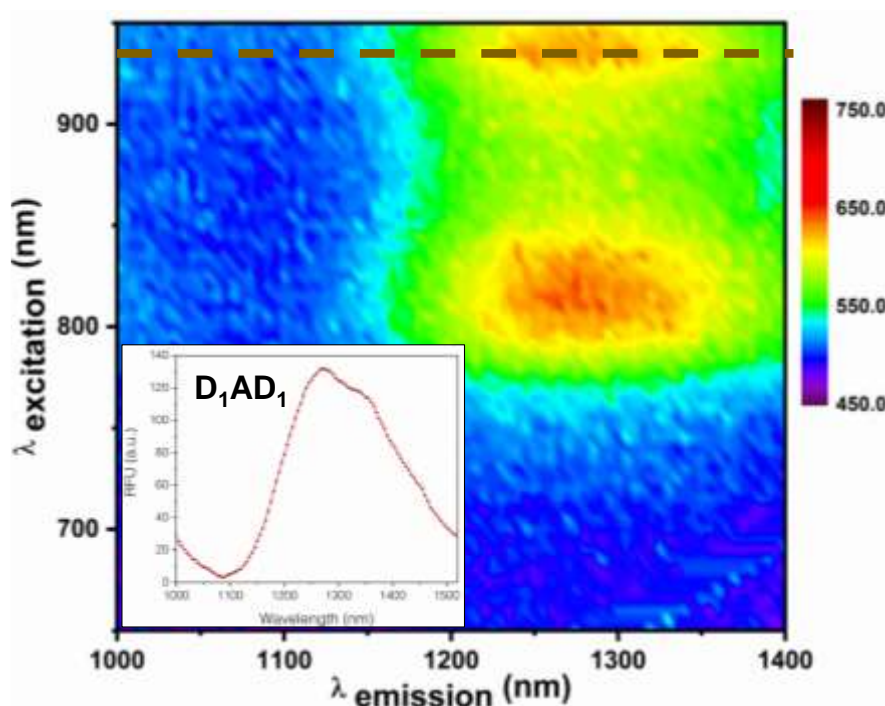


Figure S10. 2D excitation emission contour profile of D_1AD_1 dye.

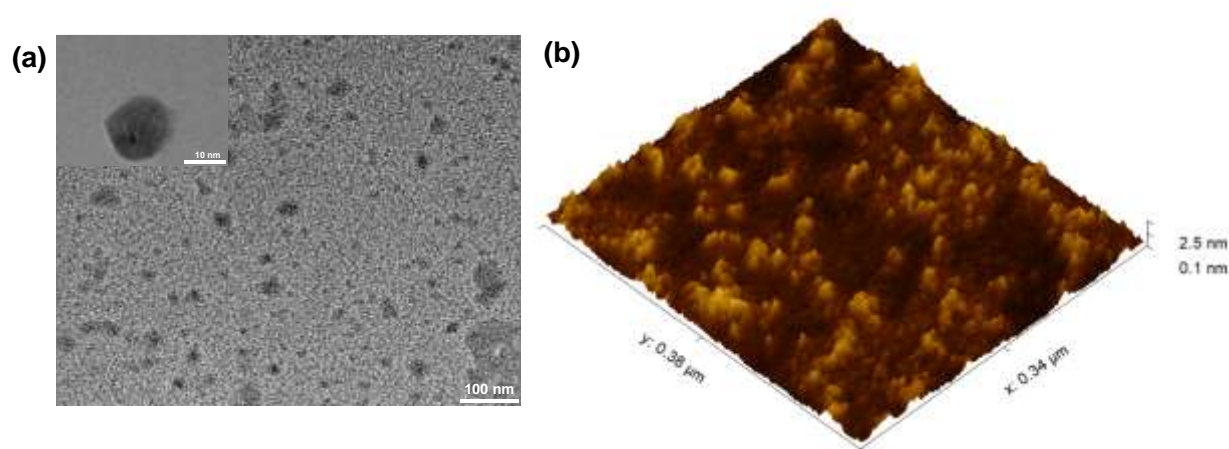


Figure S11. (a) Transmission electron microscopic and (b) atomic force microscopic images of the synthesized red carbon dots.

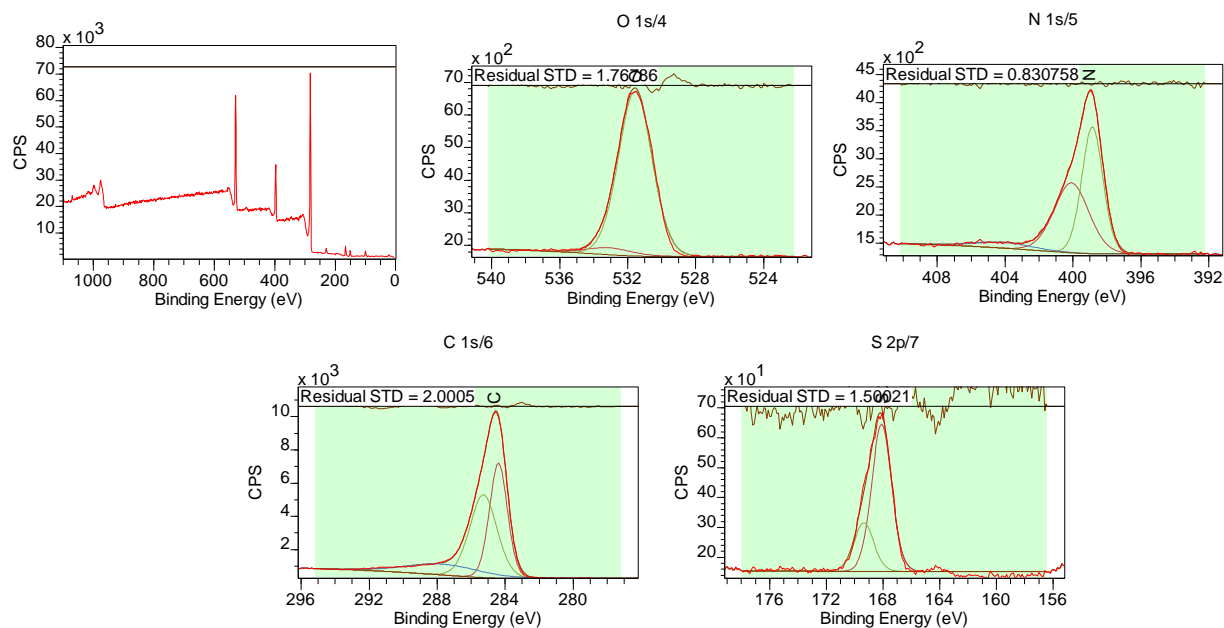


Figure S12. XPS profile for the synthesized red carbon dots.

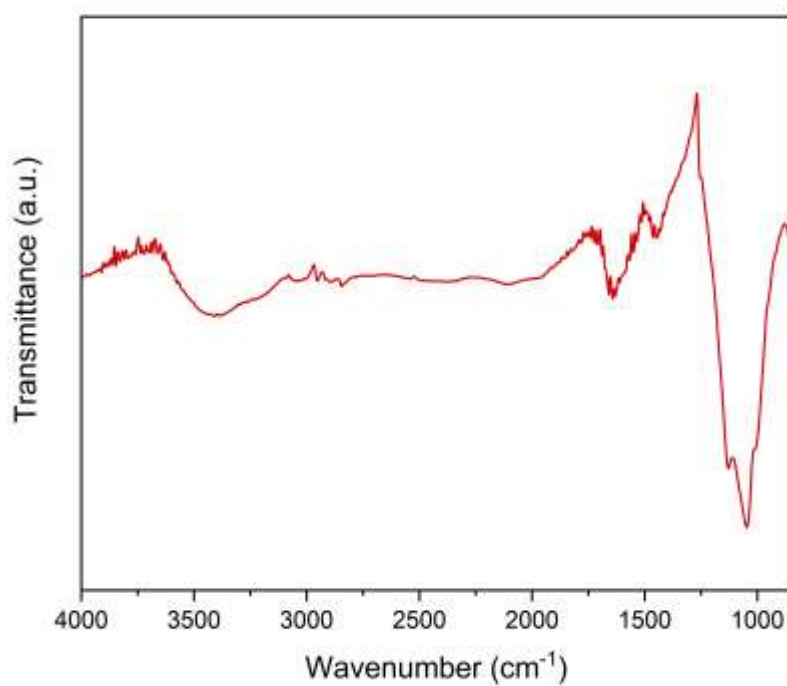


Figure S13. FT-IR spectrum of the carbon dots.

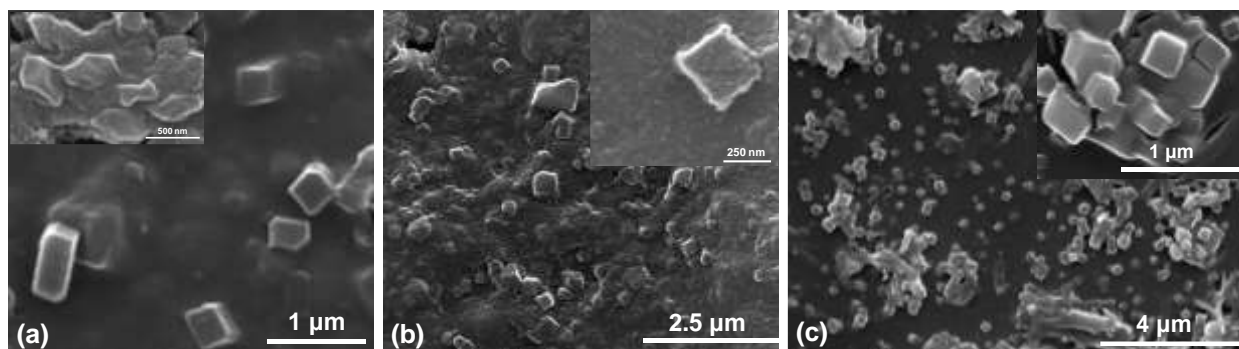


Figure S14. Scanning electron microscopic images of the carbon dot embedded host-guest complexes of (a) $D_1AD_1 \subset CB$; (b) $D_2AD_2 \subset CB$ and (c) $D_3AD_3 \subset CB$.

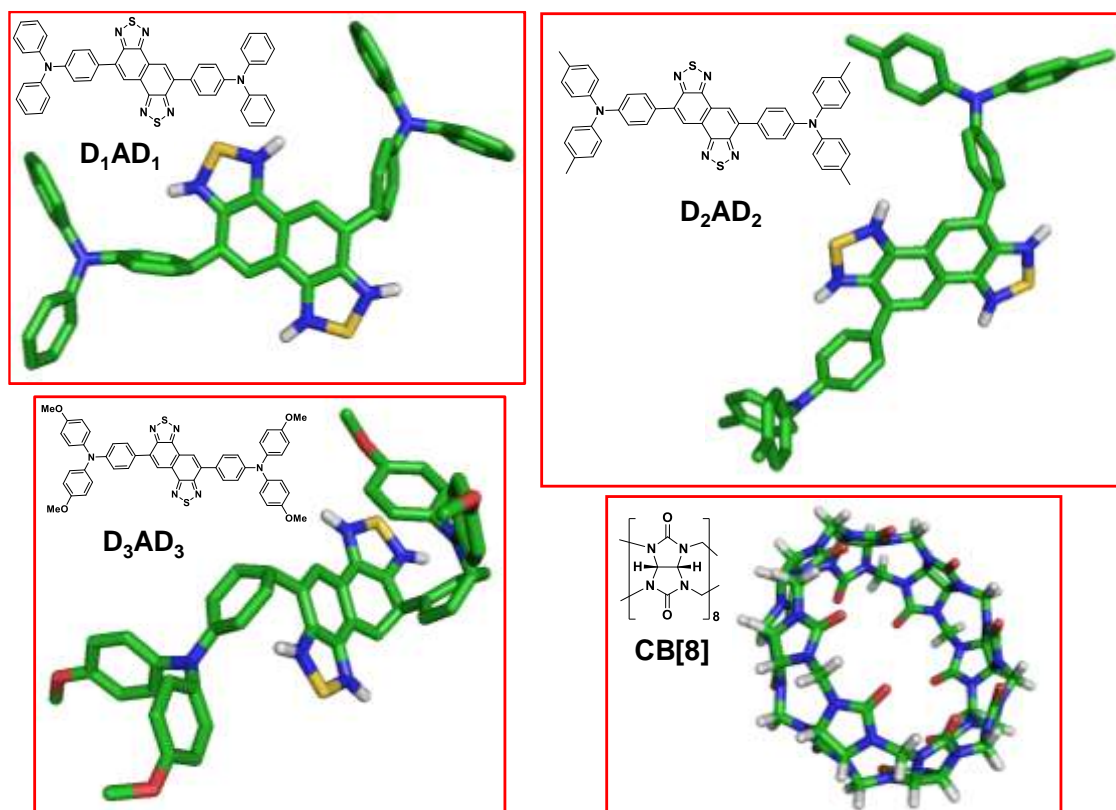


Figure S15. Energy minimized structures of D_1AD_1 , D_2AD_2 , D_3AD_3 and cucurbit[8]uril.

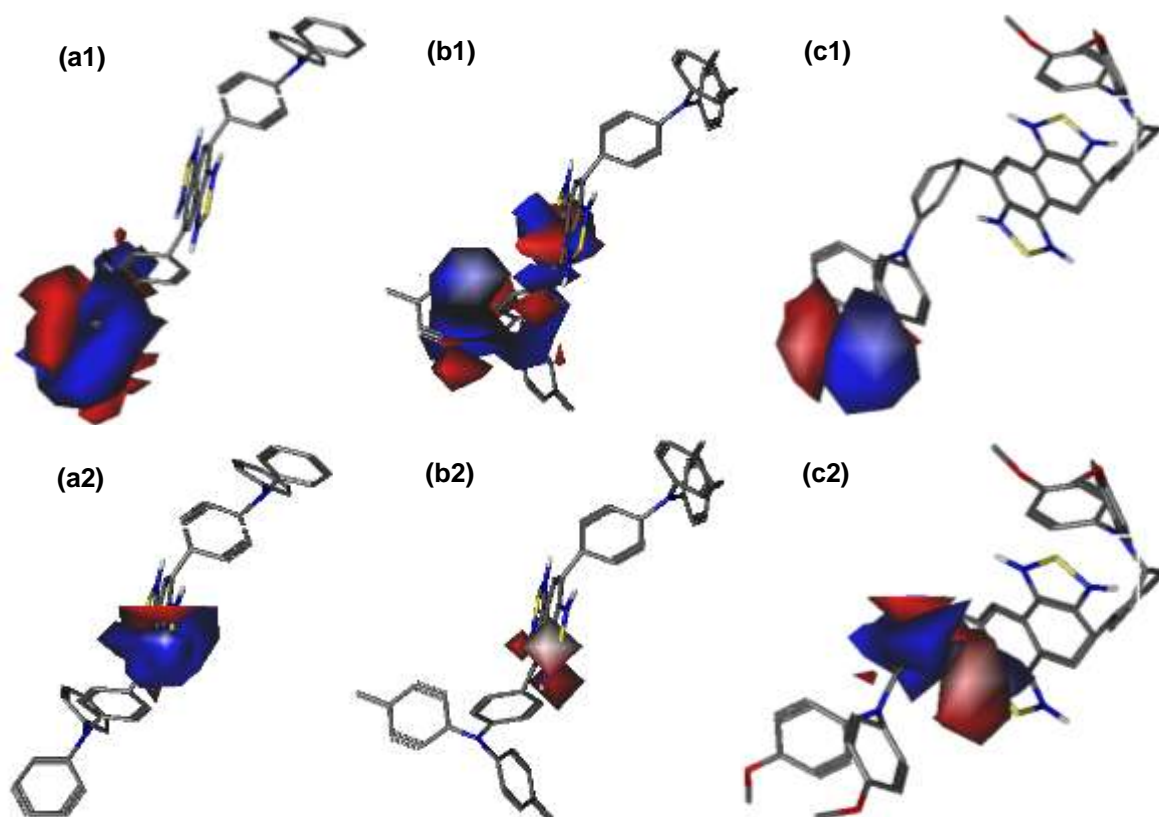


Figure S16. Pictorial diagram of (a1,b1,c1) HOMO and (a2,b2,c2) LUMO of the energy minimized structures of (a1,a2) D₁AD₁, (b1,b2) D₂AD₂ and (c1,c2) D₃AD₃.

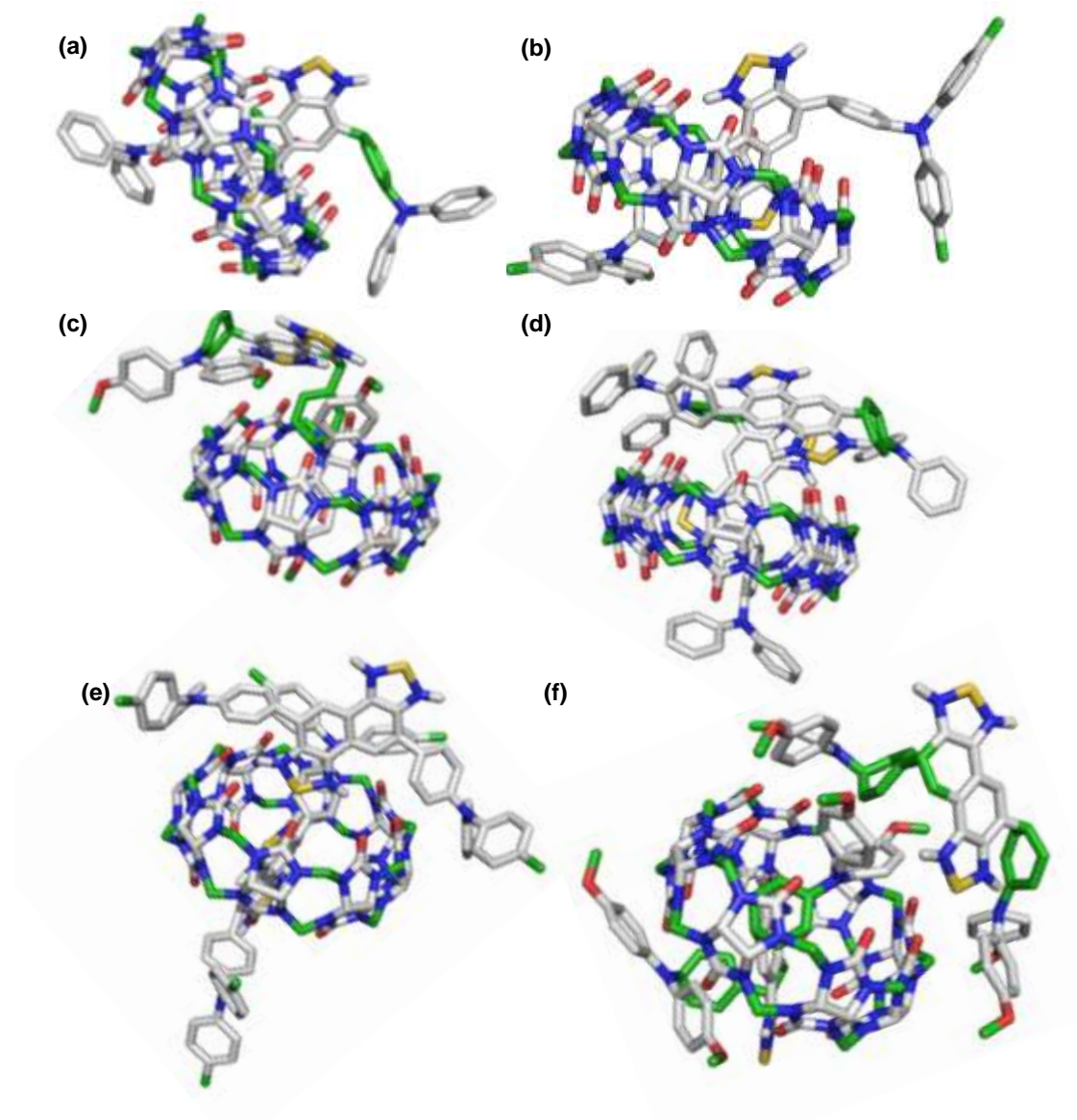


Figure S17. The most favorable docked geometries of 1:1 host-guest complexes between cucurbit[8]uril and the NIR-II dyes, *i.e.* (a) D₁AD₁; (b) D₂AD₂ and (c) D₃AD₃. The favored docked geometries for the 1:2 complexes between cucurbit[8]uril and the NIR-II dyes, *i.e.* (d) D₁AD₁; (e) D₂AD₂ and (f) D₃AD₃ were also shown.

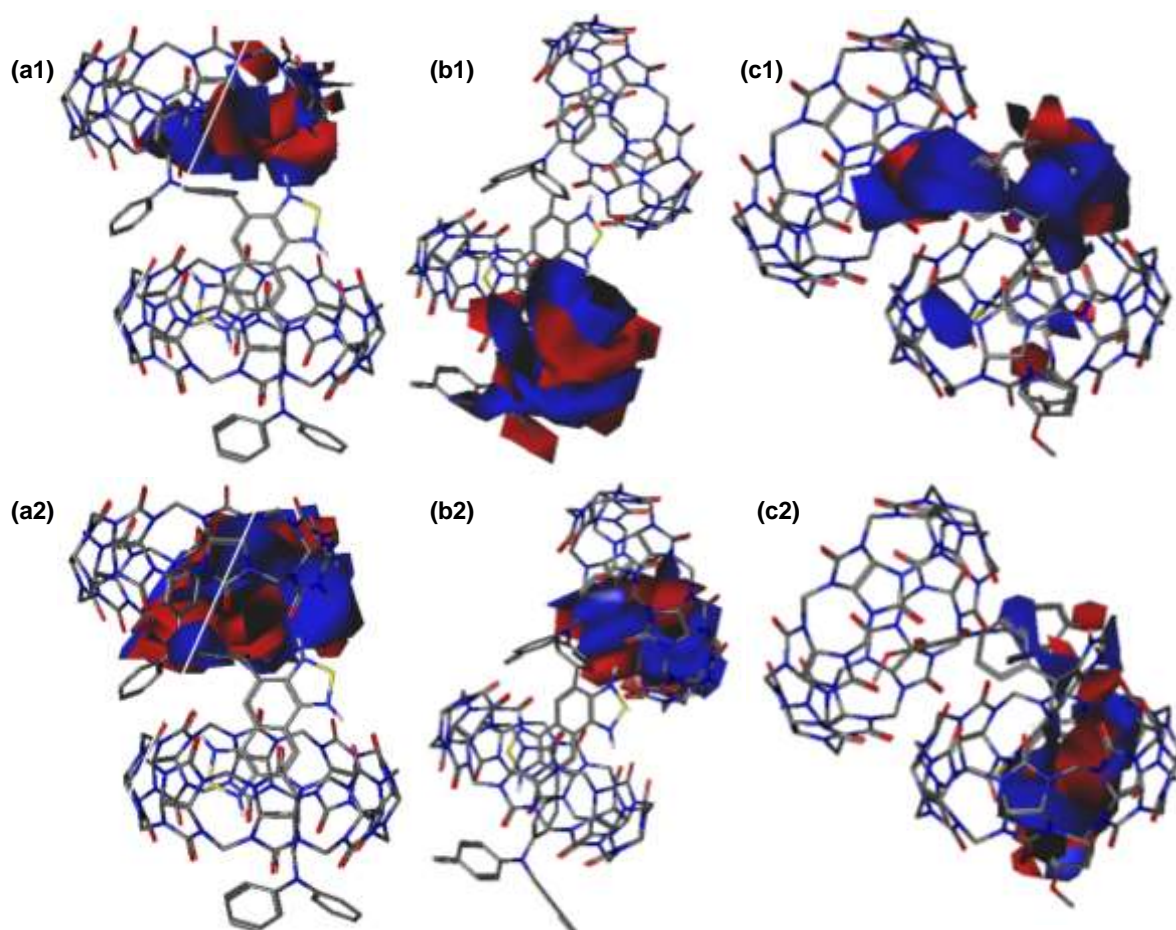


Figure S18. Pictorial diagram of (a1,b1,c1) HOMO and (a2,b2,c2) LUMO for the favored docked geometries of 1:2 host-guest complexes between the NIR-II dyes and cucurbit[8]uril respectively, *i.e.*, (a1,a2) D₁AD₁, (b1,b2) D₂AD₂ and (c1,c2) D₃AD₃.

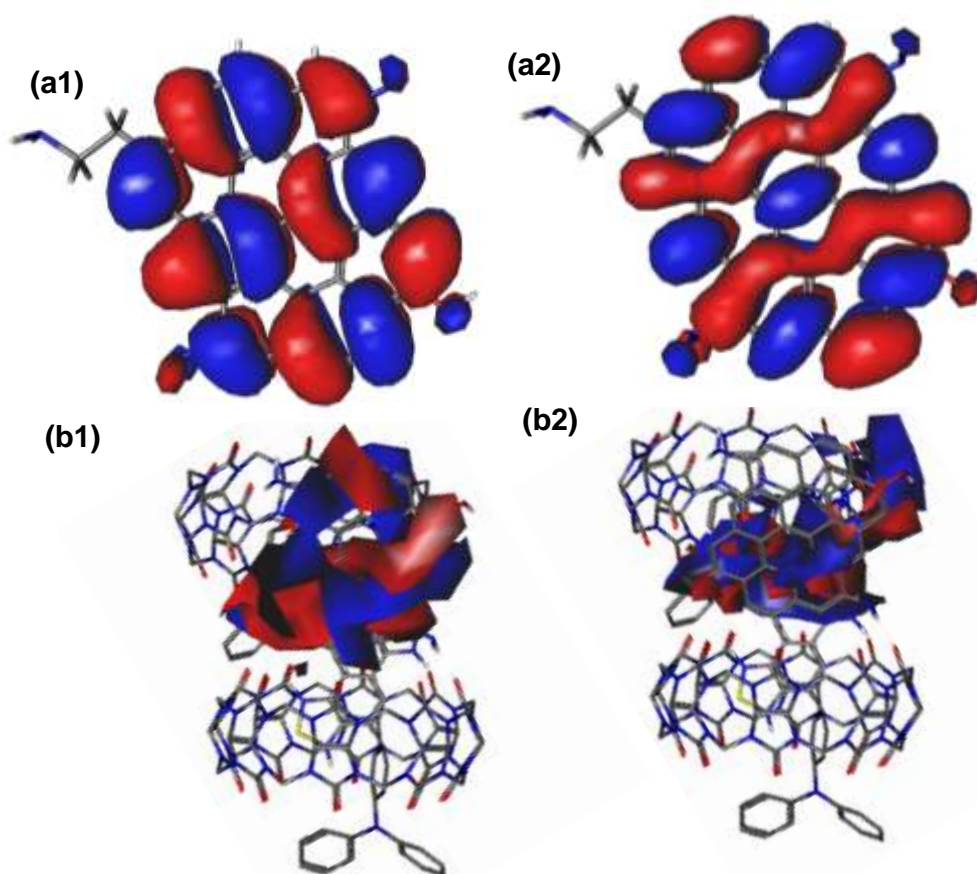


Figure S19. Pictorial diagram of (a1,b1) HOMO and (a2,b2) LUMO for the energy minimized structure of (a1,a2) model red carbon dot and (b1,b2) favored docked geometry of the supramolecularly assembled carbon dot and 2:1 host-guest complex between cucurbit[8]uril and D₁AD₁ respectively.

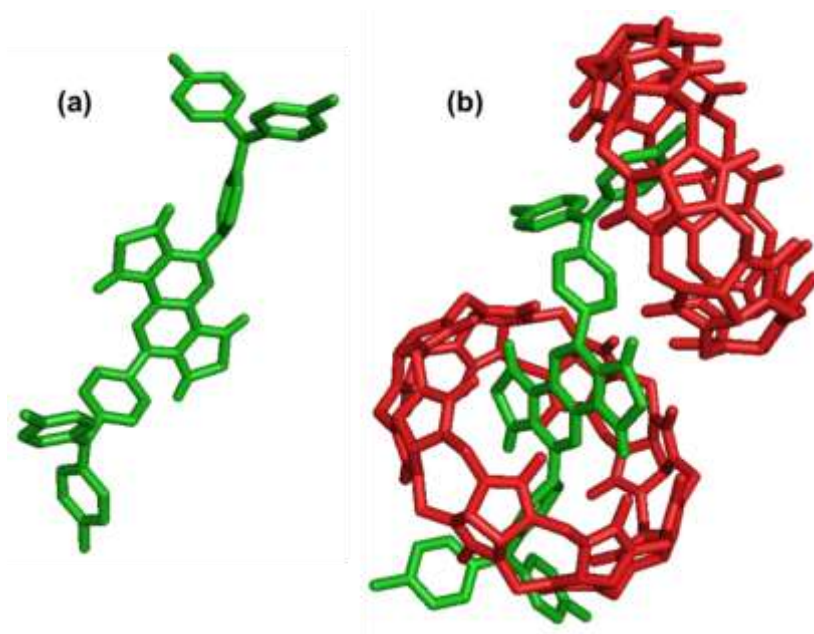


Figure S20. Representation of D_2AD_2 in (a) free state and (b) inclusion complexed state with CB[8] molecules. The dye is shown in green color and CB[8] molecules in red color.

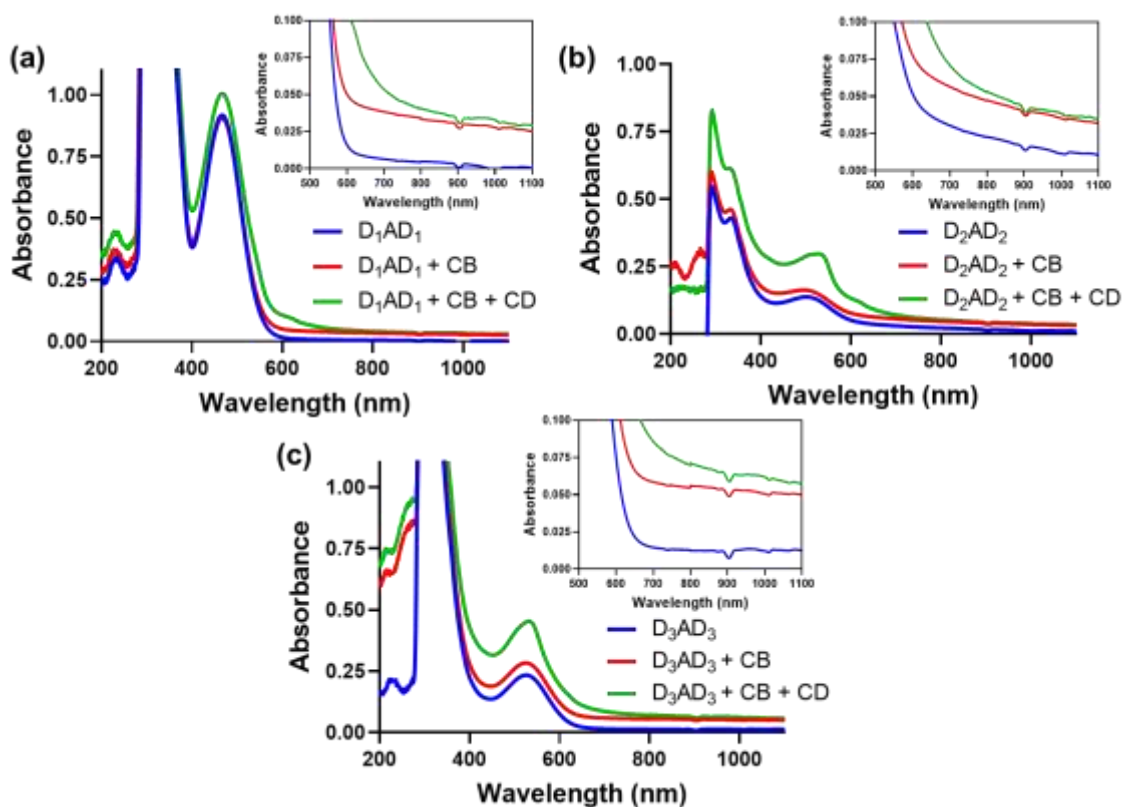


Figure S21. UV-Visible spectra of the DAD systems before and after the addition of CB and rCD. The CB and rCD conjugates with D_1AD_1 , D_2AD_2 and D_3AD_3 were shown in a, b and c respectively. Inset shows the zoom-in region from 500 to 1100 nm.

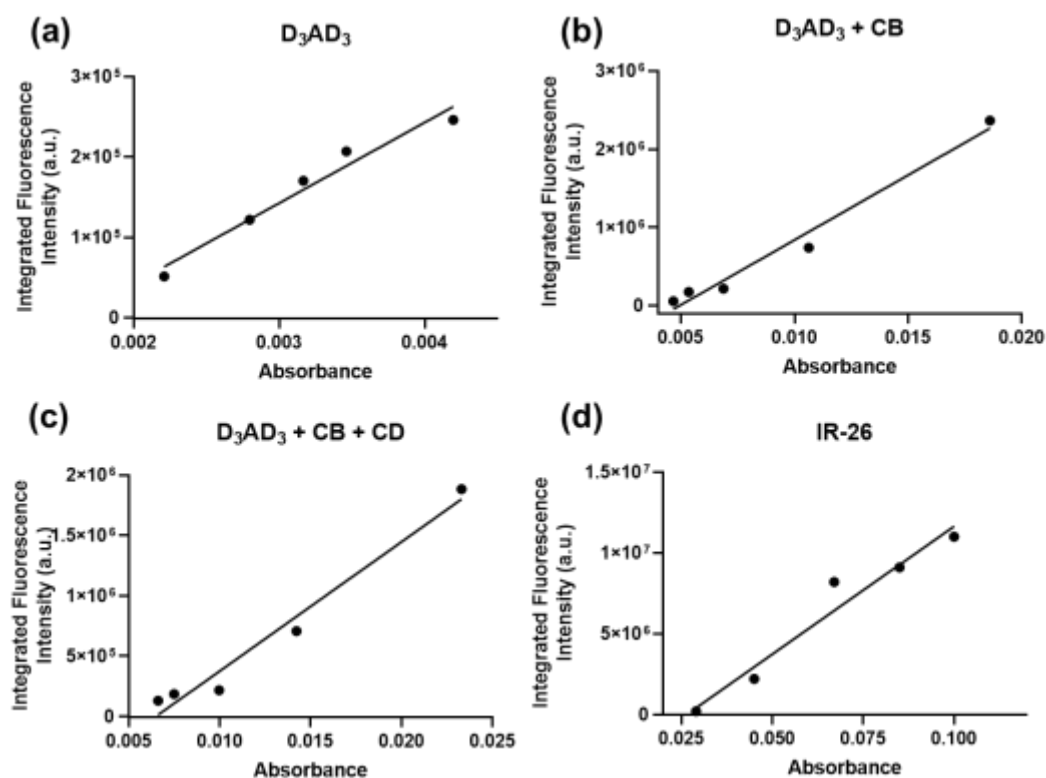


Figure S22. Plot of integrated fluorescence intensities for (a) D_3AD_3 , (b) $D_3AD_3 + CB$, (c) $D_3AD_3 + CB + rCD$ and (d) reference near-infrared fluorophore, IR-26, at five different concentrations. The slopes of the linear fits were compared to calculate the quantum yield of the conjugates. The quantum yield of IR-26 dye was referenced as 0.5%.

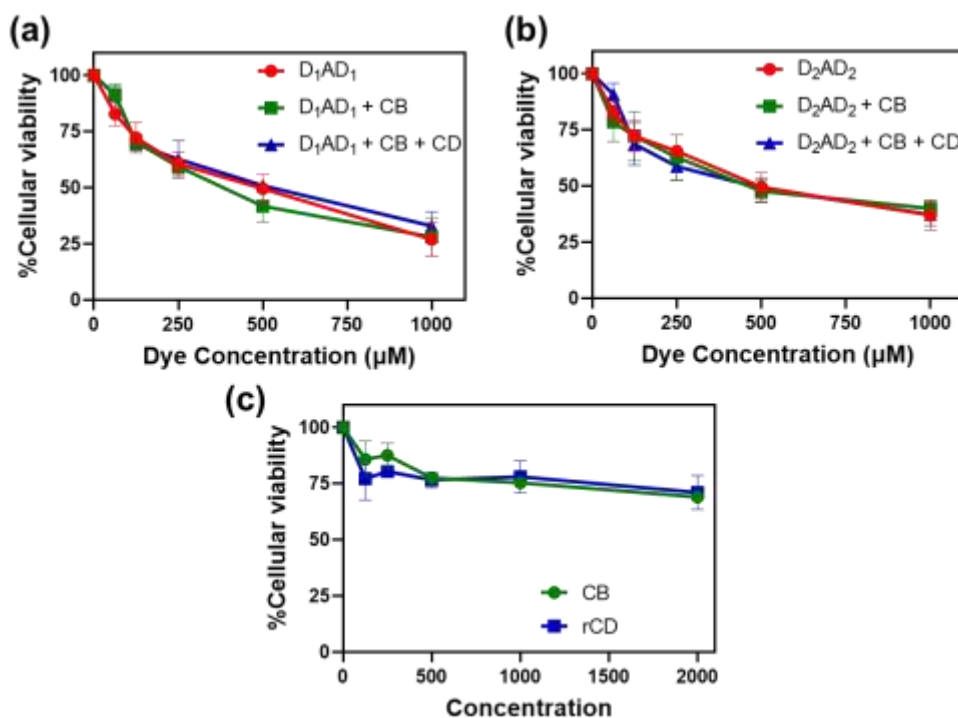


Figure S23. Comparative cellular viability of (a) D₁AD₁ and (b) D₂AD₂ conjugates before and after the addition of CB[8] and rCD in HEK293 cells. (c) The cellular toxicity of CB and rCD was also shown at different concentrations. The concentrations of CB and rCD has been represented in μM and μg/mL respectively.

Table S1. Comparative average binding energies for the host-guest complexes formed between CB[8] and NIR-II dyes, *i.e.* D₁AD₁, D₂AD₂ and D₃AD₃.

Compounds	Ratio	Average binding energy (kcal/mol))	Number of clusters among 25 different docked geometries
D ₁ AD ₁ :CB[8]	1:1	-5.168	15
D ₂ AD ₂ :CB[8]	1:1	-5.164	9
D ₃ AD ₃ :CB[8]	1:1	-4.3024	23
D ₁ AD ₁ :CB[8]	2:1	-3.5532	15
D ₂ AD ₂ :CB[8]	2:1	+22.0684	10
D ₃ AD ₃ :CB[8]	2:1	+5.1144	22
D ₁ AD ₁ :CB[8]	1:2	-5.624	1
D ₂ AD ₂ :CB[8]	1:2	-5.7988	3
D ₃ AD ₃ :CB[8]	1:2	-5.1108	3

Table S2. Clustering histogram for the 1:2 host-guest complexes between NIR-II dyes, *i.e.* D₁AD₁, D₂AD₂ and D₃AD₃, and cucurbit[8]uril with their average binding energy.

CLUSTERING HISTOGRAM

D₁AD₁:CB[8] = 1:2

Clus- ter Rank	Lowest Binding Energy	Run	Mean Binding Energy	Num in Clus	Histogram
					5 10 15 20 25 30 35
					: : : : : :
1	-5.66	5	-5.63	25	#####

Average Energy of Binding = -5.624 kcal/mol

CLUSTERING HISTOGRAM

D₂AD₂:CB[8] = 1:2

Clus- ter Rank	Lowest Binding Energy	Run	Mean Binding Energy	Num in Clus	Histogram
					5 10 15 20 25 30 35
					: : : : : :
1	-5.81	21	-5.81	10	#####
2	-5.80	20	-5.80	12	#####
3	-5.79	1	-5.78	3	###

Average Energy of Binding = -5.7988 kcal/mol

CLUSTERING HISTOGRAM

D₃AD₃:CB[8] = 1:2

Clus- ter Rank	Lowest Binding Energy	Run	Mean Binding Energy	Num in Clus	Histogram
					5 10 15 20 25 30 35
					: : : : : :
1	-5.22	16	-5.20	19	#####
2	-4.90	12	-4.85	5	#####
3	-4.78	18	-4.78	1	#

Average Energy of Binding = -5.1108 kcal/mol

Table S3. Clustering histogram for the supramolecularly assembled carbon dot embedded 1:2 host-guest complexes between the NIR-II dyes, *i.e.* D₁AD₁, D₂AD₂ and D₃AD₃, and cucurbit[8]uril with their average binding energies.

CLUSTERING HISTOGRAM					
D ₁ AD ₁ :CB[8]:rCD = 1:2:1					
Clus- ter Rank	Lowest Binding Energy	Run	Mean Binding Energy	Num in Clus	Histogram 5 10 15 20 25 30 35
1	-8.45	19	-8.34	9	#####
2	-8.35	21	-8.11	3	###
3	-7.95	25	-7.83	3	###
4	-7.81	7	-7.81	1	#
5	-7.59	15	-7.56	2	##
6	-7.53	6	-7.46	5	#####
7	-7.24	17	-7.24	1	#
8	-5.95	23	-5.95	1	#
					Average Energy of Binding = -7.85 kcal/mol
CLUSTERING HISTOGRAM					
D ₂ AD ₂ :CB[8]:rCD = 1:2:1					
Clus- ter Rank	Lowest Binding Energy	Run	Mean Binding Energy	Num in Clus	Histogram 5 10 15 20 25 30 35
1	-8.50	22	-8.35	17	#####
2	-7.85	1	-7.80	2	##
3	-7.60	12	-7.60	1	#
4	-7.60	4	-7.60	1	#
5	-7.39	5	-7.38	3	###
6	-7.12	8	-7.12	1	#
					Average Energy of Binding = -8.078 kcal/mol
CLUSTERING HISTOGRAM					
D ₃ AD ₃ :CB[8]:rCD = 1:2:1					
Clus- ter Rank	Lowest Binding Energy	Run	Mean Binding Energy	Num in Clus	Histogram 5 10 15 20 25 30 35
1	-8.15	19	-8.09	10	#####
2	-7.92	14	-7.83	12	#####
3	-7.71	21	-7.68	2	##
4	-6.91	24	-6.91	1	#
					Average Energy of Binding = -7.886 kcal/mol

3. References.

- [1] F. Ostadhossein, D. Sar, I. Tripathi, J. Soares, E. E. Remsen, D. Pan, *ACS Appl. Mater. Interfaces* **2020**, *12*, 10183-10192.
- [2] J. Walton, P. Wincott, N. Fairley, A. Carrick, *Peak Fitting with CasaXPS: A Casa Pocket Book*. 2010.
- [3] M. W. Schmidt, K. K. Baldridge, J. A. Boatz, S. T. Elbert, M. S. Gordon, J. H. Jensen, S. Koseki, N. Matsunaga, K. A. Nguyen, S. Su, T. L. Windus, M. Dupuis, J. A. Montgomery Jr, *J. Comput. Chem.* **1993**, *14*, 1347–1363.
- [4] G. M. Morris, R. Huey, W. Lindstrom, M. F. Sanner, R. K. Belew, D. S. Goodsell, A. J. Olson, *J. Comput. Chem.* **2009**, *16*, 2785-2791.
- [5] I. Srivastava, P. Moitra, D. Sar, K. Wang, M. Alafeef, J. Scott, D. Pan, *Nanoscale* **2021**, *13*, 16288.
- [6] I. Srivastava, P. Moitra, M. Fayyaz, S. Pandit, T. L. Kampert, P. Fathi, H. R. Alanagh, K. Dighe, M. Alafeef, K. Vuong, M. Jabeen, S. Nie, J. Irudayaraj, D. Pan, *ACS Applied Materials & Interfaces* **2021**, *13*, 59747.
- [7] A. L. Antaris, H. Chen, K. Cheng, Y. Sun, G. Hong, C. Qu, S. Diao, Z. Deng, X. Hu, B. Zhang, X. Zhang, O. K. Yaghi, Z. R. Alamparambil, X. Hong, Z. Cheng, H. Dai, *Nature Materials* **2016**, *15*, 235.
- [8] F. Ostadhossein, P. Moitra, N. Gunaseelan, M. Nelappana, C. Lowe, M. Moghiseh, A. Butler, N. Deruiter, H. Mandalika, I. Tripathi, S. K. Misra, D. Pan, *Nanoscale Horizons* **2022**, DOI 10.1039/D1NH00626F.